JOURNAL OF MATERIALS SCIENCE 30 (1995) 5621–5631

Effect of matrix liquid phase on interphase formation in SiC fibre-reinforced Si_2N_2O–Al_2O_3–CaO composites

HYUN-HO SHIN, Y. BERTA, R.F. SPEYER
School of Materials Science and Engineering, Georgia Institute of Technology, Atlanta, GA 30332, USA

Matrix compositions based on Si_2N_2O, with Al_2O_3 and CaO additions, were used to hot press Nicalon SiC fibre-reinforced composites at 1600 °C. With both CaO and Al_2O_3 additions, eutectic melting formed an appreciable volume of liquid phase during hot pressing, which remained as a stable glassy phase in the cooled composites. This liquid phase fostered formation of ~240 nm thick carbon-rich interphases between the fibres and the matrix. These interphases showed relatively low interfacial shear strength and resulted in composites which showed non-catastrophic, notch-independent fracture. Matrices using either Al_2O_3 or CaO did not form adequate liquid phase to form coarse interphases, and fracture was catastrophic in nature. Post-heat treatment of the composites at 1000 °C showed peripheral oxidation (removal of the carbon content of the interphase) indicating limited protection afforded when glassy phase was present in the matrix. Controlled cooling in the hot press did not cause the liquid regions to devitrify.

1. Introduction

The poor fracture toughness of monolithic ceramic materials have limited their applications; the propagation of a single crack occurs with very limited energy absorption prior to failure. Moreover, the critical strain energy release rate in mode I [1] for monolithic ceramic materials is in the range of 20–100 $J m^{-2}$, while it is ~10^4 $J m^{-2}$ for most metals [2]. Thus, critical crack sizes for ceramics are of the order of 10–100 μm, whereas those for metals are in the millimetre or centimetre range.

In order to enhance the strength and fracture toughness of ceramic materials, methods have been developed to incorporate the reinforcing media in the form of particles, platelets, whiskers, and fibres. Whisker-reinforcing has been utilized more extensively than fibre-reinforcing for practical applications to date (e.g. candidate materials for hypersonic radomes, military armour, cutting tools, and automotive engine components [3–5]), because composites with the former demonstrate isotropic mechanical properties. Uniaxial fibre-reinforcing fosters enhanced mechanical properties only in the fibre direction. The more complex design of two- or three-dimensional fibre alignment prior to matrix infiltration is required for applications where more multidirectional stresses are applied. The strain energy to failure (the area under the stress-strain curve) has been measured to be 3.1 $MJ m^{-3}$ for Nicalon SiC fibre-reinforced calcium aluminosilicate (CAS) glass-ceramic matrix composites [6]. This value is almost 40 times the strain energy to failure of the monolithic matrix material. As compared to metals such as superalloys, fibre-reinforced ceramic composites have low density, high stiffness, and high melting points. These composites show good strength and flaw tolerance as demonstrated by notch-independent fracture behaviour. They are thus potential materials for aerospace vehicles, aircraft brakes, heat exchangers, propulsion components, and space structures [3–5, 7, 8].

The non-catastropic failure of fibre-reinforced composites is due to low fibre/matrix interfacial bond energy, resulting in the debonding of fibres from the matrix [9–11], permitting crack blunting and deflection at the weak fibre/matrix interfaces [9], fibre pull-out from the matrix [12, 13], and multiple matrix cracking [14–16]. In Nicalon SiC fibre-reinforced glass/glass-ceramic composites, such low interfacial bonding is achieved by the presence of a carbon-rich interfacial layer formed between the fibre and matrix during the hot-pressing stage of composite fabrication [17].

Thus far, glass or glass-ceramic matrix composites have predominantly been fabricated by the slurry infiltration process followed by hot pressing. A low-viscosity molten phase forms in the matrix to avoid fibre damage during hot pressing [18–20]. Because the hot-press punch and die are generally made of graphite, the atmosphere surrounding the pressed composite is carbon monoxide. It has been argued [21] that this gas is molecularly soluble in the glass and reacts with the SiC fibre to form an amorphous silica and carbon product at the surface of the fibre. This product phase forms an "interphase" which is

0022–2461

credited with the low fibre/matrix interfacial bonding energy.

The problem associated with glass or glass-ceramic matrices is that in an oxidizing environment at elevated temperatures, molecularly soluble oxygen reacts with and annihilates the carbon content of the interphase [22–25] to form CO, which, in turn, diffuses out. The resulting composite shows brittle fracture behaviour. It is conceivable that if the glass phase was devitrified after matrix densification, the carbon content of the interphase regions would be protected against oxidation.

A new matrix investigated herein, the Si–Al–O–N (sialon) system, is potentially more refractory than calcium aluminosilicate and lithium aluminosilicate matrices developed in the past. These matrix compositions have been formulated based on the silicon nitride structure, with equal amounts of Al^{3+} and O^{2-} substitutions for Si^{4+} and N^{3-} in the SiN_4 tetrahedra [26, 27]. Because of its atomic arrangement, β′-sialon solid solution ($Si_{6-z}Al_zO_zN_{8-z}$ with z varying between 0 and 4) has properties which emulate Si_3N_4 – high strength and a low coefficient of thermal expansion.

With the presence of a sintering agent, e.g. CaO and MgO, an appreciable quantity of liquid phase forms during sintering of Si_3N_4. This results in the formation of a fine-grained microstructure [26] under pressureless sintering. The microstructural evolution in this system has been shown to occur by a dissolution/reprecipitation process – crystals form a eutectic liquid, which in turn precipitates a new crystalline composition, or crystals of the original composition [27]. These matrices would thus be expected to be favourable host materials for fibre-reinforcing: the liquid would foster formation of the carbon-rich interfacial layer in a similar fashion as the glass/glass-ceramic matrix, as well as minimize fibre damage during hot pressing.

2. Experimental procedure

The selected matrix compositions were 60 wt % Si_2N_2O (Norton Co., Worcester, MA)–30 wt % Al_2O_3 (Alcoa Industrial Chemicals, Bauxite, AR)–10 wt % CaO (Fisher Scientific, Fair Lawn, NJ) (coded SAC), 50 wt % Si_2N_2O–50 wt % Al_2O_3 (coded SA), and 90 wt % Si_2N_2O–10 wt % CaO (coded SC). The weighed powders were mixed and ball milled using zirconia media in water to obtain a particle-size distribution entirely less than 10 μm (diameter), as confirmed by scanning electron microscopy (SEM) observation.

The Nicalon SiC fibre tow (Nippon Carbon Co., ceramic grade SiC fibres, Tokyo), having 500 individual filaments (approximately 10–20 μm in diameter), was used as reinforcement. In the fibres, 1–3 nm SiC microcrystals and arbitrary regions of carbon aggregates were embedded in a continuum of tetrahedral SiO_xC_y $(x + y = 4)$ amorphous phase [28]. The composition of this fibre was 49% SiC, 40% C, and 11% SiO_2 in mole ratio, assuming all oxygen is tied to silicon to form SiO_2 [29]. The fibres were cut into 6 cm lengths and then heat treated in air at 350 °C for 20 min to remove a protective organic coating provided by the manufacturer. The heat-treated fibres were unidirectionally aligned in a box ($6 \times 6 \times 2$ cm^3) made of graphite foil.

A slurry was prepared by mixing powder and 2 wt % polyvinyl alcohol (PVA)/water solution using a magnetic stirrer in a closed container. The slurry was then poured into a graphite foil box containing aligned tows. The green body was immediately dried in an air-circulating oven at 120 °C for 1 h. Binder removal was accomplished by heat treating the graphite foil box containing the green body at 600 °C for 20 min in air. Hot pressing of the green body was performed in graphite dies at 1600 °C and 15 MPa in an induction-heated instrument (Alfred Enterprise Ltd, Alfred Station, NY). Carbon black powder was added around the graphite mould to protect the graphite. As a result of atmospheric oxygen reacting with the carbon black and the graphite, the atmosphere surrounding the specimens is interpreted to have been CO. The heating rate was, on average, 40 °C min^{-1}. The cooling rate after hot pressing at 1600 °C was, on average, 15 °C min^{-1} until the temperature reached 1000 °C, below which the power to the induction coil was halted and the hot-pressed composite was cooled with the die. In order to control the matrix crystallinity of the SAC and SA composition, composites were additionally fabricated using extended soaking periods and slower cooling rates (schedules 2, 3, and 4), as shown in Table I. The resultant composites contained an average of 50 vol% fibres based on SEM microstructures of the hot-pressed composite cross-section.

In order to determine the capability of the matrix to limit oxygen diffusion, composites (SAC and SA) fabricated by each schedule were post-heat treated in air at 1000 °C for 60 min. The fibre-end regions of the composites were encased in matrix, and hence fibres were not directly exposed to the environment.

For mechanical characterization, the composites were cut and polished to obtain $\sim 1.5 \times 2 \times 50$ mm^3 specimens. Three-point flexural tests (Instron Model 8562, Canton, MA) were performed for the composites fabricated by schedule 1. The span length was 4 mm and the crosshead loading rate was 0.5 mm min^{-1}. Specimen strain was taken as equivalent to crosshead

TABLE I The processing schedules and matrix compositions used at each schedule

	Schedule 1	Schedule 2	Schedule 3	Schedule 4
Soaking time at 1600 °C (min)	30	30	60	120
Cooling rate (1600–1000 °C) (°C min^{-1})	15	6	6	1
Matrix compositions	SAC, SA, SC	SA, SAC	SA, SAC	SA, SC

displacement. Apparent elastic moduli were determined based on initial tangent lines to specimen displacement versus load curves. For a highly anisotropic composite, the modulus of elasticity in bending ($N\,m^{-2}$) was determined as [30]

$$E_H = \frac{0.25L^3m}{bd^3} \quad (1)$$

where L is the support span (m), b is the width of the beam (m), d is the depth of the beam (m), m is the slope of the tangent to the initial straight-line portion of the load–deflection curve ($N\,m^{-1}$). Three specimens were tested at each composition. For the notched three-point bend test, a notch was introduced to the bend specimen geometry using a diamond saw. The notch depth (~1.25 mm) to specimen thickness (~2.5 mm) ratio was ~0.5 with a notch thickness of 0.37 mm.

Interfacial shear strength was measured via a fibre push-down test using a diamond microhardness indentor (Vickers; LECO Co., Model M-400F, St Joseph, MI). Samples were mounted in an epoxy holder and then cut to 1.8 cm lengths in the reinforced direction, followed by polishing of sample cross-sections with exposed fibre ends. As developed by Marshall and Evans [31, 32], the interfacial shear stress may be determined from

$$\tau = \frac{F^2}{4\pi^2\mu r^3 E_f} \quad (2)$$

where F is the force applied to the fibre only, r is the fibre radius, E_f is the elastic modulus of the fibre, and μ is the sliding distance through which the fibre is depressed with respect to the matrix. In determining τ, the elastic modulus for Nicalon SiC fibres in the matrix, E_f, was assumed to be 200 GPa [32]. The sliding distance, μ, was experimentally determined by the relation, $\mu = (b - a)\cot\theta$, where $2a$ is the indentation impression (diagonal distance) on the fibre, $2b$ is that on the matrix, and 2θ is the angle (136°) between opposite edges of the Vickers indentor. The diagonals $2a$ and $2b$ were measured using an optical microscope attached in the indentation instrument with a measurement precision of 0.1 μm. Part of the indentation load was supported by the matrix; to screen the matrix effect, fibres were first indented using a small load (25–50 g) to determine fibre hardness, H. Then, after full loading (100–200 g), the force on the fibre was obtained from the dimensions of the hardness impression on the fibre surface using the relation $F = a^2H/1.8544$ [33]. Fifteen fibres were indented and pushed down for 10 s for both fibre hardness and interfacial shear strength measurements. Fig. 1 shows an example of indented fibre in the SAC composite. Matrix hardness was separately measured (ten measurements for each composite) using the Vickers indentor under a 20 g load for 10 s.

Scanning electron microscopy (SEM) was used for observation of the composite fracture surfaces (AMRAY Co., Model 1810, Bedford, MA) and interfacial thickness measurements (Hitachi Ltd., Model S800, Tokyo) (ten fibre cross-sections viewed axially). Elemental analyses were performed using an attached

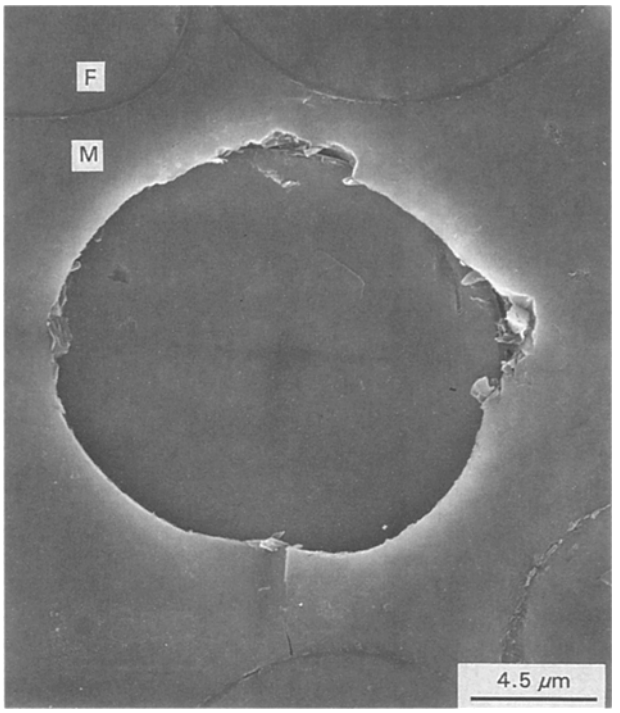

Figure 1 Indented surface of the SAC composite using a Vickers hardness indentor (under 100 g load for 10 s). Note that the interfacial layer was pushed down along with the fibre. *F*, fibre; *M*, matrix.

energy dispersive spectrometer (Kevex, Model 3600-0398, San Carlos, CA) (EDS). For a study of interfacial characteristics, transmission electron microscopy (JEOL, Model 2000FX, Tokyo) (TEM) samples were wafered into 3 mm diameter, where the radial direction of the discs were along the fibre direction. These discs were thinned mechanically to 120 μm, dimpled to 40 μm, and then argon-ion milled to electron transparency, using a liquid-nitrogen cold stage. Elemental analyses for the interfacial area were performed using an attached EDS system (Princeton Gamma Technology, Model TS16-J018, Princeton, NJ) to the TEM unit. For the detection of light elements, e.g. carbon, the beryllium window was opened during EDS data collection. As-fabricated composites were ground for X-ray diffraction (XRD) analysis (Philips Electronic

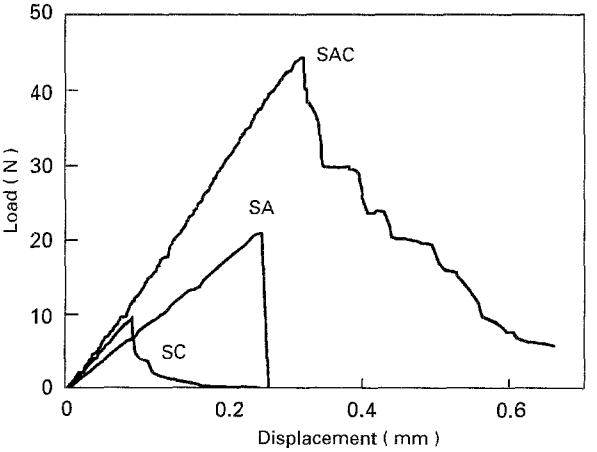

Figure 2 Typical load–displacement curves for the three-point bending of composites (fabricated by schedule 1) with the three different matrix compositions.

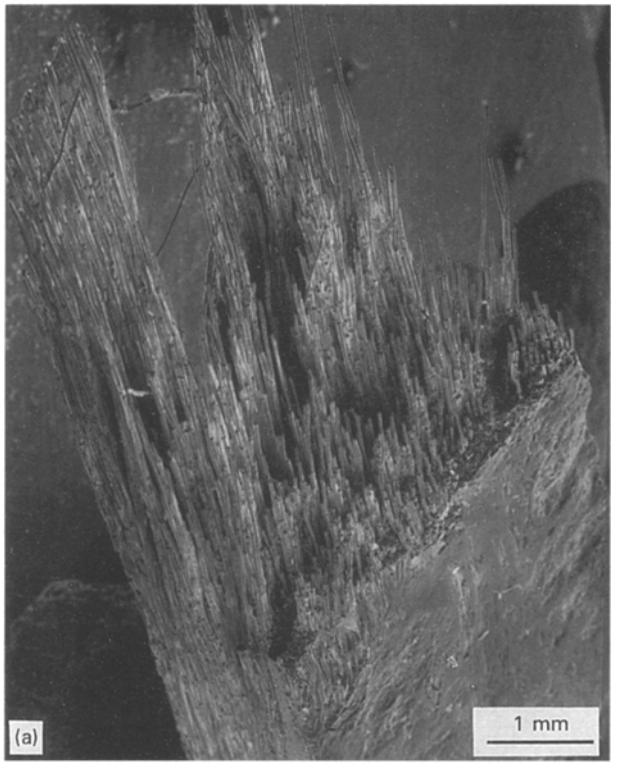

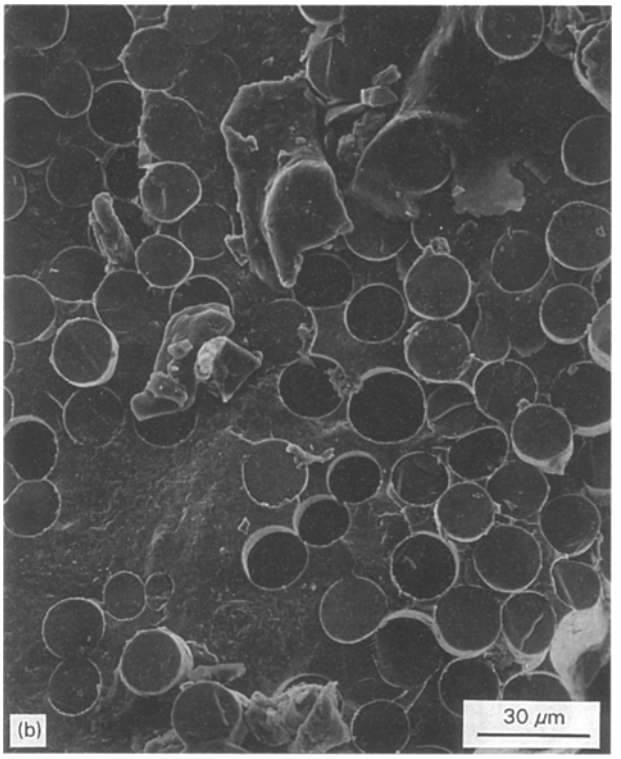

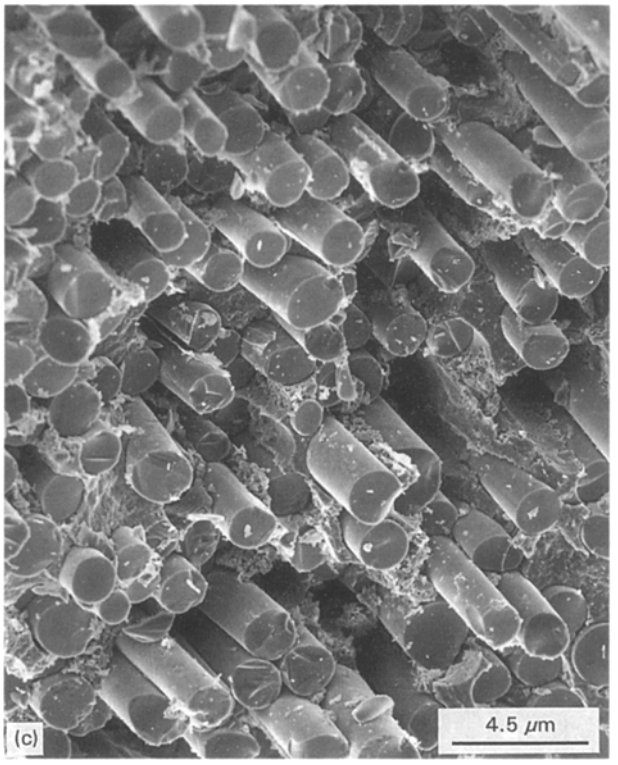

Figure 3 Fracture surfaces of (a) SAC, (b) SA, and (c) SC composites after fracture under three-point bending.

Instrument Co., Model 12045, Mount Vernon, NY, Philips, Model PW1800, Eindhoven, The Netherlands) using CuK_α radiation and a step size of 0.015°, with a duration time of 1 s at each step. Equal areas of the specimen powders were exposed to the X-ray beam.

3. Results

3.1. Mechanical behaviour

Fig. 2 shows typical flexural test for each type of composite fabricated by schedule 1. (Unless specified, all composite notations such as SAC, SA, and SC refer to the composites fabricated by schedule 1.) Non-catastrophic fracture, i.e. incremental decrease of the load with increasing deformation past the ultimate strength, was demonstrated by the SAC composite, while brittle fracture was apparent for the SA composite. Fig. 3 shows example fracture surfaces of the studied composites after three-point bending, illustrating varying degrees of fibre pull-out, depending on the matrix composition. A significant fibre pull-out in SAC, intermediate in the SC, and minimal pull-out in the SA composites were observed. Fig. 4 shows the pre-notched SAC and SA composites after three-point bending. The cracks followed the fibre direction instead of the pre-notched direction for SAC (Fig. 4a) while a catastrophic and notch-dependent fracture behaviour was demonstrated for SA (Fig. 4b). The SC composites showed a fracture behaviour similar to that of SA, but with some limited fibre pull-out on the fracture surfaces.

Flexural as well as hardness test results are summarized in Table II. Lower hardness values were measured for fibres densified in the SC matrix. Interfacial shear strengths were low in the SAC composite, higher in SC, and highest in SA. Just the opposite trend is apparent for the interphase thickness. The SAC composite showed the highest ultimate strength in bending, followed by SA, then SC. The SA composite showed a greater matrix hardness, and a lower apparent elastic modulus than the other two.

3.2. Microstructure development

Fig. 5 shows that uniform ~100 nm interphases formed between the fibres and the matrix in the SAC

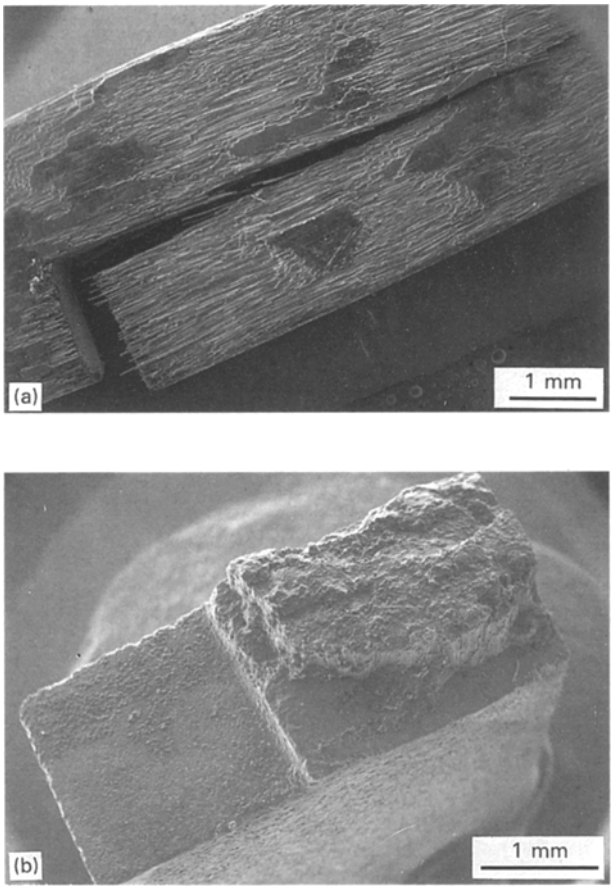

Figure 4 Fracture morphologies of pre-notched (a) SAC and (b) SA composites.

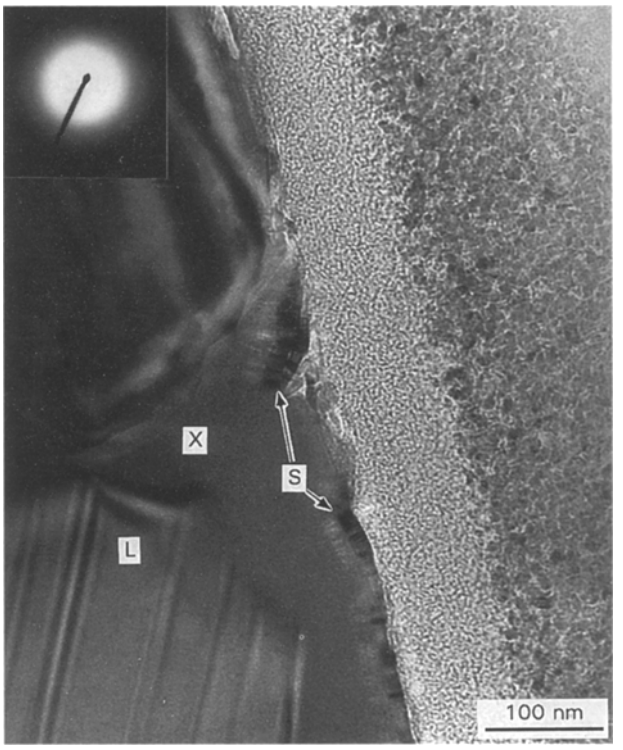

Figure 5 TEM microstructure of the SAC composite showing uniform formation of a carbon-rich interphase. The inset SAD pattern was taken from the matrix at point *X*. *S*, crystalline layer; *X*, glassy phase in the matrix; *L*, crystalline grain in the matrix.

composite. Selected-area diffraction showed that the interphase was amorphous; hence, the microstructural features within it are interpreted to be phase separation. The extinction lines in grains such as those marked L imply that they are crystalline regions. The grains in the fibre are interpreted to be SiC, while the lighter shaded grain boundaries are taken to be carbon-rich. EDS results showed that the interphase (C) contained carbon, silicon, and oxygen. The crystalline region adjacent to the interphase (area S) was rich in silicon relative to its surroundings; however, identification of this phase was not feasible. Region L showed silicon, oxygen, and nitrogen with no calcium or aluminum. Region X was comprised of silicon, aluminium, calcium, and oxygen.

Bright- and dark-field images of the SA composite are shown in Fig. 6. The interphase was thin ($\sim$35 nm) compared to that in the SAC composite (Fig. 5). The bright region in the dark-field image indicates that the phase in contact with the interphase was crystalline. EDS showed that the oval grain in the SA matrix was composed of silicon, and oxygen while the matrix around the grain was made up of silicon, aluminium and oxygen. Other regions (not shown) surrounding grains of similar form to the oval grain were amorphous (by selected-area diffraction), and also were composed of silicon, aluminium and oxygen. Fig. 7 illustrates the interphase which formed in the SC composite. Crystalline regions can be seen within the interphase. EDS results imply that these regions were calcium-rich relative to the surrounding amorphous interphase. The calcium content in the fibre centre was higher than fibre centres in the SA and SAC composite

TABLE II Summary of the measured mechanical properties of the composites fabricated by schedule 1. ± values represent standard deviation

	Matrix composition		
	SAC	SA	SC
Fibre hardness (GPa)	14.9 ± 1.0	14.8 ± 1.2	12.9 ± 0.7
Interfacial shear strength (MPa)	30.8 ± 13.8	170.1 ± 48.7	100.9 ± 31.8
Matrix hardness (GPa)	11.3 ± 1.6	16.3 ± 0.9	12.1 ± 1.4
Interphase thickness (nm)	238.7 ± 35.3	38.9 ± 13.5	131.4 ± 45.6
Three-point bend strength (MPa)	438.7 ± 31.4	228.0 ± 17.8	151.9 ± 17.2
Three-point elastic modulus (GPa)	146.6 ± 18.1	82.9 ± 20.5	131.3 ± 11.6

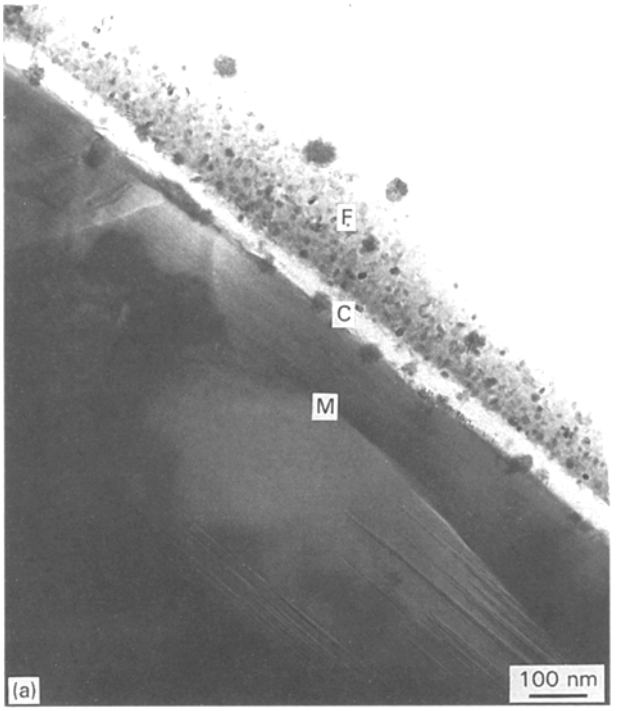

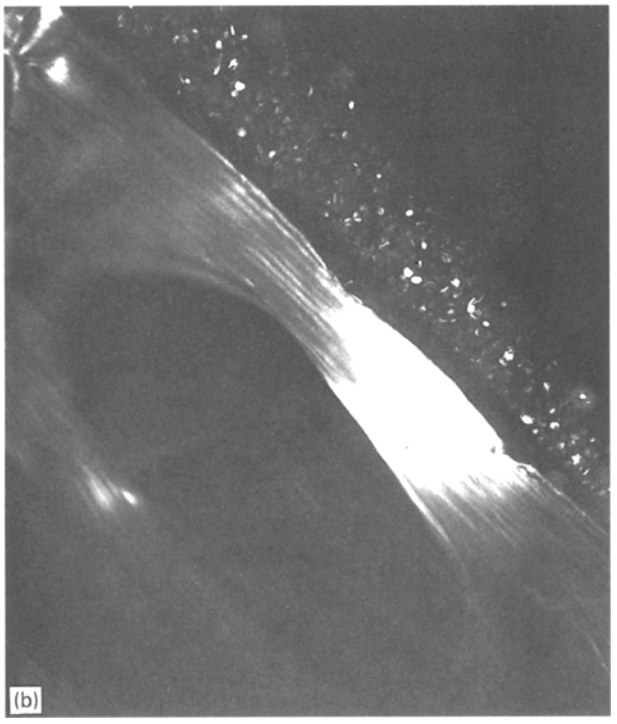

Figure 6 (a) Bright-field image of the SA composite showing a thin (~35 nm) interphase. *F*, fibre; *C*, interphase, and *M*, matrix. (b) Dark-field image of the same area showing that the matrix phase in contact with the interphase was also crystalline. Spots on the interphase and fibre are due to contamination during specimen thinning.

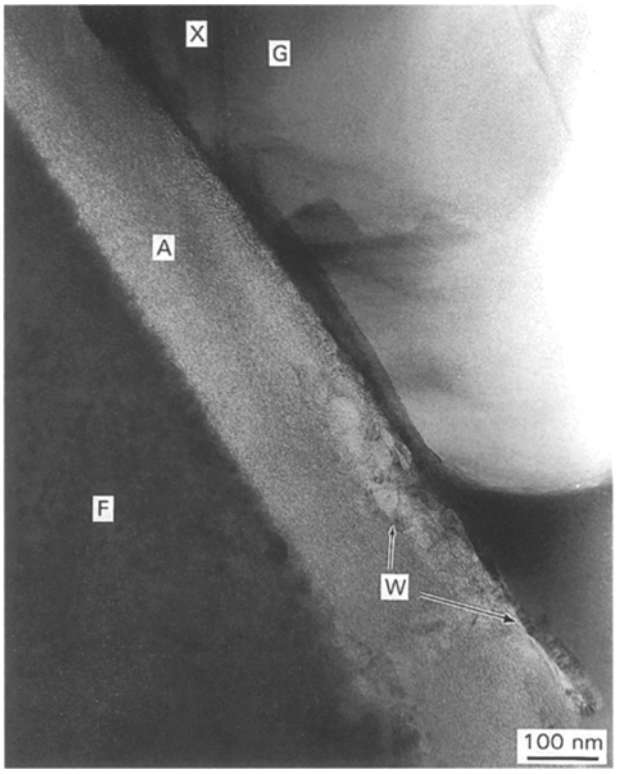

Figure 7 TEM microstructure of the SC composite. *G*, amorphous matrix region; *X*, crystalline matrix region; *F*, fibre; *A*, amorphous interphase region; *W*, crystalline interphase region.

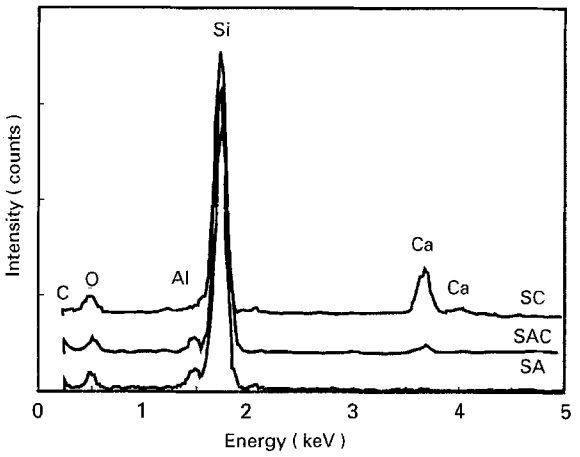

Figure 8 EDS of fibre centres for the three composites. EDS peaks were normalized to the silicon peak intensity.

(Fig. 8). Fig. 9 shows the insufficient matrix densification in the SA composite. The SAC and SC composites were nearly pore free.

XRD patterns of ground composites are shown in Fig. 10. The SAC and SC composite patterns showed Si_2N_2O as the only crystalline phase present. Si_2N_2O, Al_2O_3 and a sialon-X phase [34] (composition: $Si_{12}Al_{18}O_{39}N_8$ [35], $Si_3Al_6O_{12}N_2$ [36], or $Si_2Al_3O_7N$ [37]) were identified for the SA composite. XRD patterns of the SAC composites fabricated by each schedule are shown in Fig. 11. Alumina showed the most intense presence after schedule 3, while it was only possibly present after schedules 2 and 4. The relative intensities of Si_2N_2O did not show a consistent trend with schedules. Mullite showed a minor presence after schedule 4. Peaks matching the JCPDS database for β'-Si_3N_4 were identified; however, they are expected to represent those of β'-sialon solid solution. Fig. 12 shows XRD patterns of the SA composites fabricated by each schedule in Table I. The sialon-X phase disappeared with extended high-temperature exposure, and was replaced by mullite ($Al_6Si_3O_{11}$).

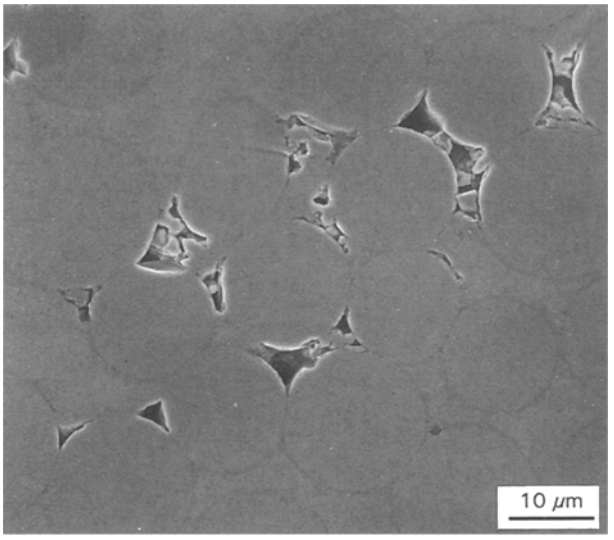

Figure 9 Insufficient matrix densification in the SA composite.

The microstructure of a post-heat treated (at 1000 °C for 1 h in air) SAC composite is shown in Fig. 13. Fibre pull-out was observed on the fracture surface only at the central portion of the composite (Fig. 13a). Fig. 13b shows circumferential holes at fibre/matrix interfaces with a number of bridges between fibres and the matrix. Composites fabricated by schedules 2, 3, and 4 did not show any apparent differences from the circumferential oxidation behaviour shown in Fig. 13. This oxidation behaviour was observed for SA and SC composites as well.

4. Discussion

Under schedule 1, the only remaining matrix crystalline phase in SAC was Si_2N_2O. This phase represents unreacted relic particles, where all other Si_2N_2O reacted to extinguish alumina and calcia, forming a eutectic liquid. The composition of the liquid phase permitted its retention as a stable glass with cooling in the hot press; in the presence of Ca^{2+}, two Al^{3+} ions can adopt two Si^{4+} network (glass-former) positions. With increasing time at elevated temperatures in the hot press (schedules 2–4), the liquid phase partially devitrified forming mullite. The formation of β′-sialon is interpreted to be a reaction product of Si_2N_2O relic and the liquid phase. Slow cooling in the hot press did not cause full devitrification of the amorphous phase. EDS showed no indication of nitrogen in the glass. Without a significant overpressure of nitrogen, the solubility of nitrogen in the liquid phase would be low.

In the SA composite, eutectic melting between Si_2N_2O and Al_2O_3, formed a liquid phase which enveloped residual silicon oxynitride grains. Without charge-compensating alkaline earth cations (e.g. Ca^{2+}), all Al^{3+} cations would take network modifier positions, forming three non-bridging oxygens for every aluminium ion. Hence, the alumina-rich supercooled aluminosilicate liquid phase was not stable, and devitrified to form sialon-X. Because the liquid phase in SA would be more alumina-rich than that in SAC, the more alumina-rich sialon compound (sialon-X) would form in favour of the generally more silica-rich β′-sialon. With longer hot-pressing schedule, sialon-X was extinguished in favour of mullite. This implies that sialon-X represents a metastable phase.

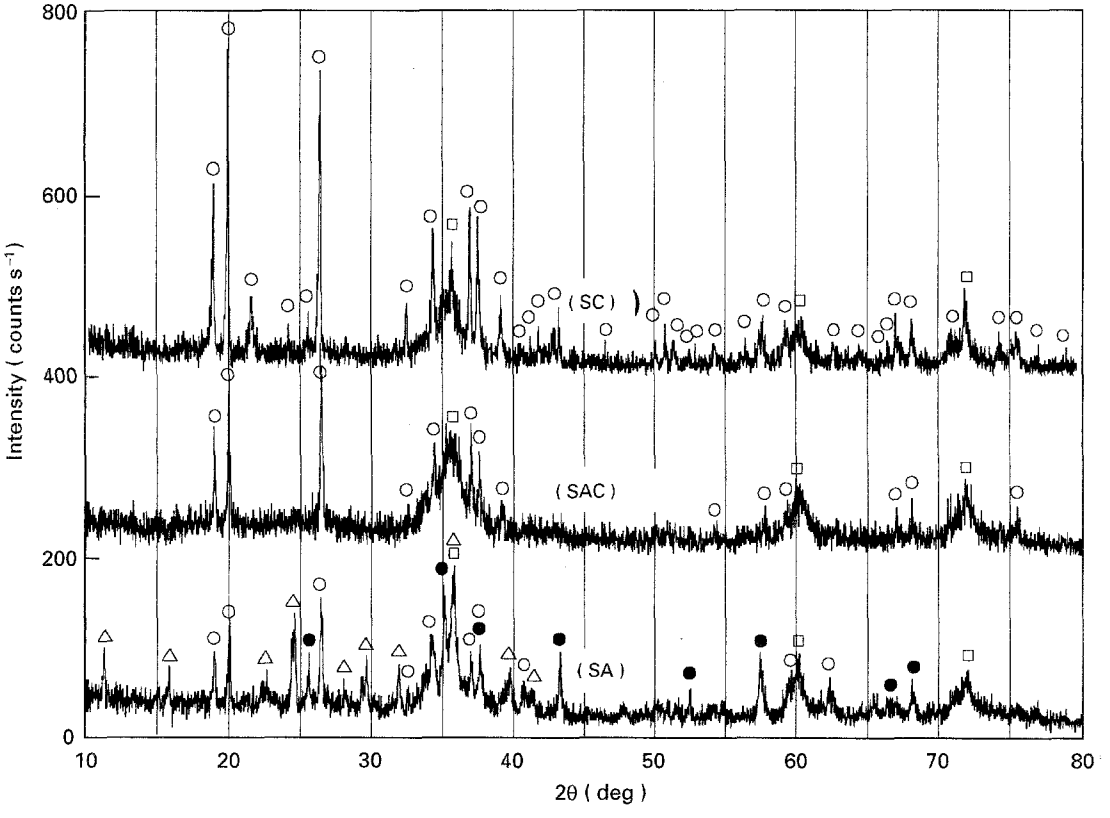

Figure 10 XRD patterns for the three composites. (○) Si_2N_2O, (△) sialon-X, (●) Al_2O_3, (□) β-SiC.

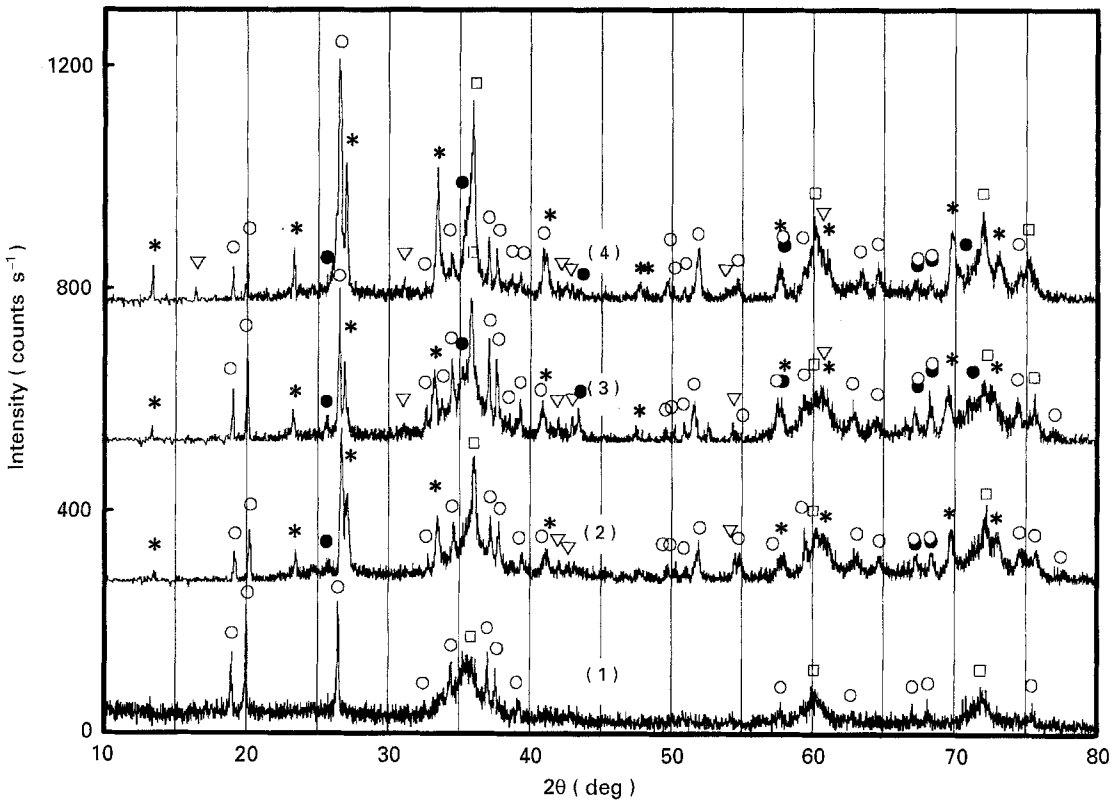

Figure 11 XRD patterns from the SAC matrix composites hot pressed under schedules indicated in Table I. The XRD trace for schedule 1 was taken on a different diffractometer, using a different sample stage than for schedules 2, 3 and 4. (○) Si_2N_2O, (●) Al_2O_3, (▽) $Al_6Si_2O_{11}$, (*) β′-Si_3N_4, (□) β-SiC.

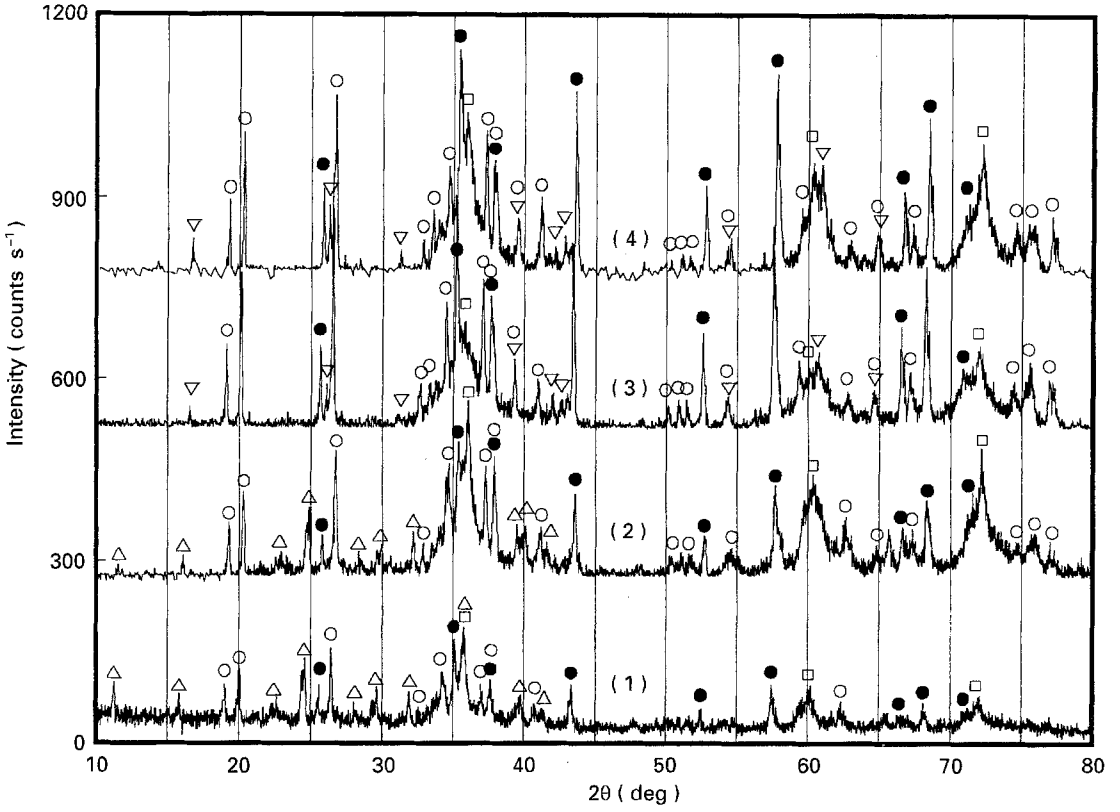

Figure 12 XRD patterns from the SA matrix composites fabricated by schedules 1, 2, 3, and 4. See note in Fig. 11 regarding diffractometers. (○) Si_2N_2O, (●) Al_2O_3, (▽) $Al_6Si_2O_{11}$, (△) sialon-X, (□) β-SiC.

With time at elevated temperature, the lack of a high nitrogen overpressure may have fostered a solid state, or solution and precipitation transformation, liberating nitrogen to the surroundings.

The SC composite also formed an amorphous phase under schedule 1, because a calcium silicate liquid (with a low proportion of calcium) forms a stable glass. A lower percentage of glassy phase would be expected

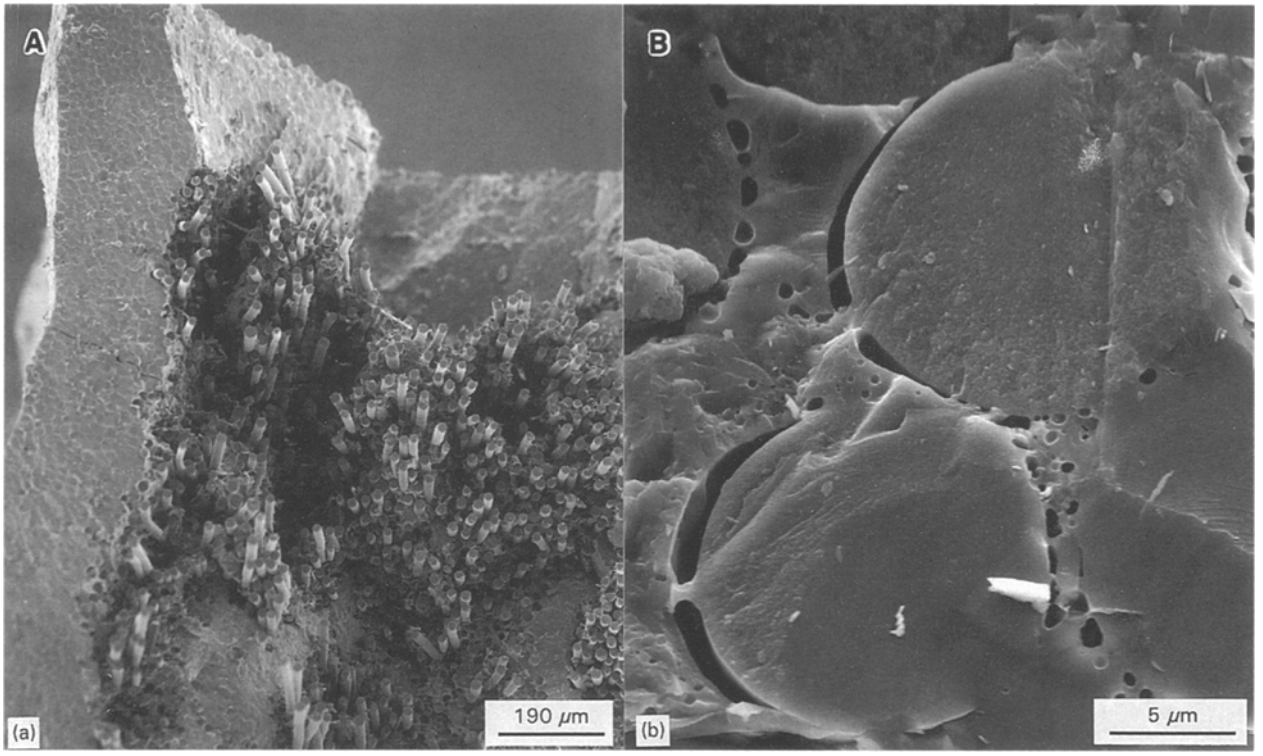

Figure 13 (a) SEM microstructure of the fracture surface of post-heat treated (at 1000 °C for 1 h in air) SAC composite. (b) Magnified view of the outer portion of the composite where no fibre pull-out was observed.

in SC as compared to SAC, because in SC there was only 5.75 mol% CaO to react with Si_2N_2O. Comparing the liquid phases formed in SC and SAC composites, it would be expected that for a given temperature, the calcium aluminosilicate glass in SAC would be more viscous than the calcium silicate glass in SC. The more fluid SC liquid phase is interpreted to have encouraged chemical interaction between the matrix, interphase and fibre. This is indicated by the calcium-containing crystalline phases in the interphases and the high calcium content in the fibres.

Complete matrix densification in the SA composite did not occur (Fig. 9). This implies that the tenure of liquid phase prior to devitrification to sialon-X was short, which would impede full densification via liquid-phase infiltration of pores. The high porosity shown in Fig. 9 correlates to the lower elastic modulus of this composite due to the lower cross-sectional area available to resist the applied load [38].

The formation of the interphase is related to conditions which are adequately oxidizing to form silica and carbon from SiC, but not oxidizing enough to form CO or CO_2. Oxidizing agents can be provided by pre-existing oxygen between particles in the compact, or can be gases which diffuse in between the hot press die and punch. Based on the reaction $SiC + O_2 = C + SiO_2$ [39], the volume of molecular oxygen at 1 atm required to form a 0.3 μm thick interphases in a standard specimen is calculated to be 1139 cm^3. This calculation was based on a carbon density of 1.2 $g\,cm^{-3}$ and amorphous silica density of 2.5 $g\,cm^{-3}$. This volume is much greater than the composite volume of 18 cm^3, hence, interphase formation by reaction with trapped oxygen in the pre-hot-pressed green body is negligible. Thus, diffusion of soluble carbon monoxide gas through the matrix is taken as the dominant mechanism of interphase formation [40].

Interphase formation appears to be closely related to the presence/absence of fluid phase in the matrix during densification. This is consistent with the results of other investigations. A carbon-rich interphase was commonly observed between SiC whiskers and a glass-ceramic matrix [41] while no layer formed with a polycrystalline Al_2O_3 matrix [42], where no appreciable fluid phase would have formed during densification. Molecular solubility of gases would be appreciably higher in liquids than in solids. Hence, it would be expected that interphases in SA and SC would be underdeveloped because of the comparatively deficient volume of liquid phase during hot pressing. In SAC, the interphase thicknesses at fibre-sparse areas were observed to be greater than at the fibre-rich area.

If interphase thickness is not interpreted to be a factor in the mechanical properties of the composite, the lower ultimate bending strength of SA, relative to SAC, may be related to the high-porosity matrix. The pores acted as stress concentrators, increasing matrix cracking for a given load as compared to a more well-densified matrix such as SAC. However, the interfacial shear strength of SA was measured to be significantly higher than SAC. Further, the fracture morphology of SA showed minimal fibre pull-out. These results imply that the low interphase thickness promoted crack propagation through the fibre, rather than debonding. The relative contributions of either phenomenon to the lowered ultimate strength has not

been established. The enhanced calcium content in the SC fibre clearly altered its properties as indicated by the drop in fibre hardness in this composite. The low ultimate strength of this composite is interpreted to be a result of loss of structural integrity of the fibres along with high interfacial shear strength due to underdeveloped interphases.

The circumferential holes (Fig. 13) formed at the fibre/matrix interface of the SAC composite after heat treatment in air are interpreted to be caused by the oxidation of the carbon content of the interphase by molecularly soluble oxygen in the amorphous portions of the matrix ($2C_{(s)} + O_{2(glass)} = 2CO_{(glass)}$). The bridges formed between the holes would have been the remaining amorphous SiO_2 in the interphase, mixed with other matrix oxides to form a calcium aluminosilicate glass. Similar oxide glass bridges were observed with a lithia aluminosilicate system [43]. This oxidation process undoubtedly also oxidized the fibres, reducing their cross-sectional area. The fibre pull-out at the central portion of the SAC composite indicates a time-dependent diffusion of molecular oxygen to various interphase locations, and diffusion of CO out to the composite surface.

5. Conclusion

The SAC matrix composition formed a considerable quantity of liquid phase, which in turn fostered the development of $\sim$240 nm thick carbon-rich interfacial layers of relatively low interfacial shear strength ($\sim$30 MPa). The fracture behaviour of the resultant composite was non-catastrophic and notch-independent. SA and SC matrix compositions formed microstructures containing less glassy phase, formed thin interfacial layers (39–131 nm), and had higher interfacial shear strengths. These composites showed catastrophic fracture with limited fibre pull-out. SC composites formed a liquid phase which allowed calcium infiltration into the interphase and fibre, worsening the mechanical properties of the composite. The presence of liquid phase in the matrix permitted diffusion of CO to react with the fibre to form the interphase. There was no evidence that the amorphous matrix phases contained nitrogen. With extended periods in the hot press, and nitrogen-bearing crystalline phases such as sialon-X were annihilated in favour of oxide phases (mullite), but the resulting composites were still comprised of partly vitreous matrices. Post-heat treatment of all composites at 1000 °C showed peripheral oxidation and removal of the carbon content of the interphases.

Acknowledgements

The authors thank Dr Chen Park for TEM operation which led to Fig. 5. Much of this work was performed while the authors were with the New York State College of Ceramics at Alfred University, Alfred, NY.

References

1. D. BROEK, "Elementary engineering fracture mechanics", 4th Revised Edn (Kluwer Academic, Boston, 1991).
2. M. R. PIGGOTT, "Load-bearing fiber composites" (Pergamon Press, New York, 1980).
3. S. J. GRISAFFE, *Adv. Mater. Process.* **137**(3) (1990) 43.
4. *Idem, ibid.* **137**(3) (1990) 93.
5. J. R. STEPHENS, *ibid.* **137**(4) (1990) 35.
6. R. SORENSEN, PhD thesis, Technical University of Denmark (1993).
7. S. AWASTHI and J. L. WOOD, *Ceram. Eng. Sci. Proc.* **9** (1988) 553.
8. W. E. COLE, P. REAGAN, C. I. METCALFE and S. R. WYSK, *ibid.* **8** (1987) 968.
9. J. COOK and J. E. GORDON, *Proc. R. Soc.* **A282** (1964) 508.
10. A. G. EVANS, M. Y. HE and J. W. HUTCHINSON, *J. Am. Ceram. Soc.* **72** (1989) 2300.
11. P. G. CHARALAMBIDES and A. G. EVANS, *ibid.* **72** (1988) 746.
12. A. H. COTTRELL, *Proc. R. Soc.* **A282** (1964) 2.
13. H. C. CAO, E. BISCHOFF, O. SBAIZERO, M. RUHLE, A. G. EVANS, D. B. MARSHALL and J. J. BRENNAN, *J. Am. Ceram. Soc.* **73** (1990) 1691.
14. J. AVESTON, G. A. COOPER and A. KELLY, in "Properties of Fiber Composites", National Physical Laboratory Conference Proceedings, edited by National Physical Laboratory (IPC Science and Technology Press, Guildford, UK, 1971) pp. 15–26.
15. J. AVESTON and A. KELLY, *J. Mater. Sci.* **8** (1973) 352.
16. B. BUDIANSKY, J. W. HUTCHINSON and A. G. EVANS, *J. Mech. Phys. Solids* **34** (1986) 167.
17. J. HOMENY, J. R. VAN VALZAH and M. A. KELLY, *J. Am. Ceram. Soc.* **73** (1990) 2054.
18. K. M. PREWO, in "Proceedings of the Conference on Tailoring Multiphase and Composite Ceramics", edited by R. E. Tressler, G. L. Messing, C. G. Pagano and R. E. Newnahm (Pennsylvania State University, Plenum, NY, 1985) pp. 529–47.
19. K. M. PREWO, J. J. BRENNAN and G. K. LAYDEN, *Am. Ceram. Soc. Bull.* **65** (1986) 305.
20. *Idem, Ibid.* **65** (1986) 322.
21. H. H. SHIN, Y. BERTA and R. F. SPEYER, in "Advances in ceramic composites", Ceramic Transactions Vol. 38, edited by N. P. Bansal (American Ceramic Society, Columbus, OH, 1993) pp. 235–48.
22. T. MAH, M. G. MENDIRATTA, A. P. KATZ, R. RUH and K. S. MAZDIYASNI, *J. Am. Ceram. Soc.* **68** (1985) C-248.
23. E. Y. LUH and A. G. EVANS, *Ceram. Eng. Sci. Proc.* **6** (1986) 608.
24. E. Y. LUH and A. G. EVANS, *J. Am. Ceram. Soc.* **70** (1987) 466.
25. M. D. THOULESS, O. SBAIZERO, E. BISCHOFF and E. Y. LUH, *Mater. Res. Soc. Symp. Proc.* **120** (1990) 333.
26. K. H. JACK, in "Non-oxide technical and engineering ceramics", edited by S. Hampshire (Elsevier Applied Science, New York, 1986) pp. 1–30.
27. K. H. JACK, *Mater. Res. Soc. Symp. Proc.*, **287** (1993) 15.
28. C. LAFFON, A. M. FLANK, P. LAGARDE, M. LARIDJANI, R. HAGEGE, P. OLRY, J. COTTERET, J. DIXMIER, J. L. MIQUEL, H. HOMMEL and A. P. LEGRAND, *J. Mater. Sci.* **24** (1989) 1503.
29. G. SIMON and A. R. BUNSELL, *ibid.* **17** (1982) 2371.
30. "Standard Test Methods for Flexural Properties of Unreinforced Plastics and Electrical Insulating Materials: D790–91", Annual Book of ASTM Standards (American Society for Testing and Materials, Philadelphia, PA, 1991).
31. D. B. MARSHALL and A. G. EVANS, *J. Am. Ceram. Soc.* **68** (1985) 225.
32. D. B. MARSHALL, *ibid.* **67** (1984) C-259.
33. Reference manual for the Vickers indentor, Model M400-F, LECO Co., St Joseph, MI.
34. A. ZANGVIL, L. J. GAUCHKLER and M. RUHLE, *J. Mater. Sci.* **15** (1980) 788.
35. I. K. NAIK, L. J. GAUCKLER and T. Y. TIEN, *J. Am. Ceram. Soc.* **61** (1978) 332.

36. G. K. LAYDEN, "Process Development for Pressureless Sintering of SiAlON Ceramic Components," Final Technical Report R75-91072-4, United Technologies Research Center, East Hartford, CT (1976).
37. A. W. J. M. RAE, D. P. THOMPSON and K. H. JACK, in "Ceramics for high performance applications", Vol. II, edited by J. J. Burke, E. N. Lenoe and R. N. Katz (Brook Hill, Chestnut Hill, MA, 1978) pp. 1039–67.
38. R. L. COBLE and W. D. KINGERY, *J. Am. Ceram. Soc.* **39** (1956) 377.
39. R. F. COOPER and K. CHYUNG, *J. Mater. Sci.* **15** (1980) 463.
40. P. M. BENSON, K. E. SPEAR and C. G. PANTANO, *Ceram. Eng. Sci. Proc.* **9** (1988) 663.
41. V. S. R. MURTHY, L. JIE and H. LEWIS, *ibid.* **10** (1989) 938.
42. R. BARRETT and T. F. PAGE, *ibid.* **10** (1989) 897.
43. H. H. SHIN and R. F. SPEYER, *J. Mater. Sci.* **29** (1994) 3630.

Received 22 December 1994
and accepted 15 March 1995